Journal of Asian Earth Sciences
September 2022, Volume 235, Pages 105298 (12p.)
https://doi.org/10.1016/j.jseaes.2022.105298
https://archimer.ifremer.fr/doc/00772/88424/

Deformational pattern and seismogenic potential of the eastern Makran subduction zone

Parvaiz Shaukat [1, 3, *], Ali Aamir [1], Javed Farhan [2], Ali Shah Muhammad [2]

[1] Department of Earth Sciences, Quaid-i-Azam University, 45320, Islamabad, Pakistan
[2] Centre for Earthquake Studies, National Centre for Physics (NCP), Islamabad, Pakistan
[3] Department of Geological Engineering, Balochistan University of I.T, Engineering and Management Sciences (BUITEMS), Quetta, Pakistan

* Corresponding author : Shaukat Parvais, email addresses : parvaiz_geo@hotmail.com ; Shaukat.Parvaiz@buitms.edu.pk

Abstract :

In last 500 years, the ~900 km long Makran subduction zone (MSZ) has hosted 9 M7+ large earthquakes, and 8 of them activated the eastern segment of the fault. The 1945 M 8.1 megathrust event also generated significant tsunami signifying the region as active subduction zone in the world. Here, we investigate the deformation patterns and seismogenic potential of MSZ utilizing detailed seismic data analyses. Mechanical modeling based on limit analysis approach has also been applied to better understand the seismic shaking potential of ongoing deformation and retrieve the associated frictional properties. The seismic structural interpretation illustrates that MSZ has an imbricate thrust fault system. Furthermore, seismic attributes highlight the fractured and high porosity zones, which reduce friction values along the plate interface. The estimated effective friction to slip does not exceed 0.12 along the subduction interface. We found that ~0.04-0.12 is required to reproduce the observed fault system. For wedge geometry, we run different simulations to measure the frontal horizontal and vertical slip. Assuming the convergence rate of 3-4 cm/yr, the calculated slip deficit in last 77, 158, and 257 years, after 1945, 1864 and 1765 earthquakes along offshore-ruptured patches of eastern MSZ is 2.31-3.08 m, 4.74-6.32 m, and 7.71-10.28 m, respectively. A frontal uplift ranging from 0.69 ± 0.37 to 3.02 ± 1.45 m can be expected, if the next rupture occurs along the previously ruptured areas, which possess the ability to amplify the water column and generate a large tsunami in the region.

Graphical abstract

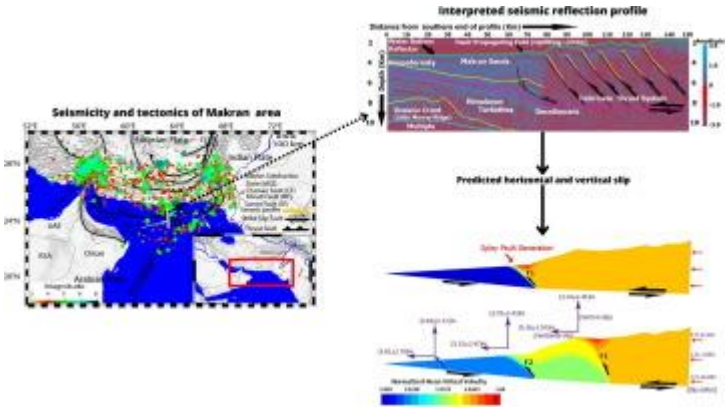

Highlights

► The Makran subduction zone has an imbricate thrust fault system. ► Attribute analyses show Makran turbidities are fractured under high pore pressures. ► Lateral continuity is observed in the frontal region via velocity analysis. ► Effective friction 0.04-0.12 is required to reproduce the observed fault system. ► Splay faults with high uplift values can amplify earthquake related tsunami.

Keywords : Deformation pattern, Seismogenic/seismic shaking potential, Imbricate thrust fault system, Seismic attributes, Mechanical modeling, Limit Analysis

1. Introduction

In the Makran region, the Arabian plate subducts beneath the Eurasian plate in the southern coasts of Iran and Pakistan at a rate of 3-4 cm/yr over an approximately 900 km margin. Convergence rate increases from 3 cm/yr in the west to 4 cm/yr in the east (Byrne et al., 1992; DeMets et al., 1994; Kopp et al., 2000; Smith et al., 2012). The Makran Accretionary Wedge (MAW) grows seaward as a result of this subduction at a probable rate of 1 cm/yr (Ahmed, 1969; White, 1982; Platt et al., 1985). The Makran subduction zone (MSZ) connects to the Zagros thrust system through Minab dextral fault and the southern Chaman sinistral fault system in the west and east, respectively (Figure 1). This subduction zone extends up to a triple junction in the west of Karachi, Pakistan, where the Arabian, Eurasian, and Indian plates meet. The MSZ (Arabia/Eurasia motion), the transtensional Murray Ridge system (India/Arabia motion), and the Chaman transform fault system (Eurasia/India motion) connect at this triple junction.

In addition to extensive fault systems, the MSZ has produced the world's largest arc-trench gap i.e., 500-600 km (Flueh et al., 1997) and accretionary wedge system. This system stretches from a deformational front nearly 150 km offshore to a wide volcanic zone 200-300 km onshore in Pakistan and Iran, characterized by thick sedimentary strata of more than 7 km (Minshull et al., 1992; Kopp et al., 2000). Moving 70 km seaward of the forearc region, more recent accreted, unconsolidated, and semi-consolidated sediments under high pore fluid pressures and low seismic velocities can be observed (Byrne et al., 1992). More than half of the Makran accretionary wedge (MAW) is exposed in the onshore region, introducing a sequence of imbricate thrust fault system in a north-south direction (Minshull et al., 1992; Priestley et al., 2022; Figure 1).

Gravity modeling supports the concept of a low angle dip of the Arabian plate under the Eurasian plate in the Makran area (White, 1979). The seismic reflection data interpretation (through MAW) revealed

that the MSZ has a shallow (i.e., ≤ 8º) dip angle (Harms et al., 1984, Kopp et al., 2000; Schluter et al., 2002, Penney et al., 2017, Priestley et al., 2022). In this largest active wedge having thick sediment sequence of more than 7 km, the rocks are youngest at the coast and become older to the north (Ahmed, 1969; Raza et al., 1981; Farah et al., 1984; Kopp et al., 2000). The most dominant image at the top of the oceanic crust utilizing seismic reflection profile CAM-30 allows us to determine the thickness of MAW and its over thrusting (Figure 2a, b).

Jackson and McKenzie (1984) proposed that almost all subduction earthquakes arise at shallow depth i.e., <20 km. In case of MSZ, the seismicity is also shallower (located at depths up to 20 km in offshore area) (Heidarzadeh et al., 2008; Penney et al., 2017; Burg, 2018). However, overall more recent moderate size seismicity at intermediate depth (50-100 km) have demonstrated the intraslab seismicity in the onshore region of Makran (Jacob and Quittmeyer, 1979; Laane and Chen, 1989; Byrne et al., 1992; Maggi et al., 2000; Pararas-Carayannis, 2006; Rajendran et al., 2013; Penney et al., 2017; Priestley et al., 2022). According to Byrne et al. (1992), Rajendran et al. (2013), Lin et al., (2015) and Abedi and Bahroudi (2016) the eastern and western Makran have different seismicity, with a boundary at the Pakistan/Iran border. In addition, only Makran offshore region has experienced at least six large earthquakes (M>7) rupturing the plate boundary in the last 500 years (namely 1483, 1765, 1851, 1864, 1945, 1947) (Heidarzadeh, 2011; Lin et al., 2015; Figure 1). The active nature of MSZ earthquakes has been widely studied (e.g., Page et al., 1979; Quittmeyer and Jacob, 1979; Ambraseys and Melville, 1982; Byrne et al., 1992; Penney et al., 2017). Additionally, most recent destructive earthquakes in the onshore area include 2011 M7.3 Dalbandin and 2013 M7.7 Awaran (Balochistan) earthquake.

The large shallow subduction earthquakes mostly generate tsunamis in the coastal region (Satake and Tanioka, 1999), but sufficient deformation produced by deeper earthquakes to cause tsunami is rarely observed (Scawthorn and Chen, 2002). The MSZ has generated a devastating tsunami in 1945 as a result of M8.1 earthquake. Moreover, MSZ has a splay fault deformation pattern with active seismogenic

potential and long recurrence intervals for major earthquakes (>M8). Within an accretionary wedge, splay faults are relatively weak zones that rupture often during subduction earthquakes (Park et al., 2002). For example, in 1944 M8.1 Tonankai, 1946 M8.3 Nankai, 1960 M9.2 Chilean, 1964 M9.0 Alaskan, and 2004 M9.2 great Sumatra-Andaman earthquakes, the strong influence of splay fault on tsunami wave height in the near-field was observed (Heidarzadeh, 2011). Heidarzadeh (2011) further elaborated that splay faults are steeply dipping thrust faults that branch upward from the subduction zone to the seafloor and are also known as imbricate faults. Splay faults are capable of causing substantial seafloor deformation, which can considerably enhance tsunami heights in the near field because of their high dip angles (Aslam et al., 2021).

Here, we investigate the deformation style and its seismic shaking potential for the Makran subduction megathrust and its splay faults. According to Hassani et al. (1997), Lamb and Davis (2003) and Bonnardot et al. (2008), frictional characteristics define the mechanical coupling of the subduction interface which may impact the stress state, deformation pattern, and uplifting of the continental margin. The seismic potential of the subduction megathrust can be better understood by modeling the frontal wedge, which has a lot of internal deformation. Similarly, examination of the mechanical state and structural analysis of the frontal wedge helps in understanding its response to seismic shaking (Byrne et al., 1988; Ruff and Tichelaar, 1996; Fuller et al., 2006; Wang and Hu, 2006). To conduct structural imaging of the MSZ, we have used seismic reflection profiles passing near the epicenter of the 1945 M8.1 earthquake. To describe the frictional characteristics of megathrust and imbricate fault system, we have applied limit analysis approach for mechanical modeling. The study will help to better understand the tsunamigenic potential of this subduction zone and its impact on the seismic and tsunami hazard of the region.

2. Material and methods

2.1 Pre-existing data

The R/V Marion Dufresne (a German based company) surveyed Pakistan's Makran accretionary wedge in 2004. Prior to this survey, the German R/V Sonne collected some geophysical and swath bathymetric data during cruises SO90, SO122, SO123, SO124, and SO130 (Kukowski et al., 2000). During the Makran and Murry Traverse (MAMUT') survey (SO123) in 1997 (Kopp et al., 2000), wide-angle seismic data was obtained to complete the earlier seismic reflection data, which was surveyed by the Bullard Laboratories of Cambridge group in 1986 (White, 1979; White and Louden, 1982; Minshull and White, 1989; Minshull et al., 1992).

2.2 Seismic data interpretation

We choose two seismic profiles from two distinct surveys passing through the same area to study the deformation pattern of frontal MAW (Figure 1). The seismic profile CAM-30 (Minshull et al., 1992) from the Cambridge Group survey (Figure 2a-b) is a post stack depth migrated multichannel seismic profile, whereas the seismic profile SO123-08 (https://oceanrep.geomar.de/id/eprint/27136/) from the German R/V Sonne survey is a single channel wide-angle seismic reflection profile (Figure 2c). Both seismic profiles are overlapping throughout the wedge but deviates maximum 5 km from each other in Oman abyssal plain (Flueh et al., 1997; Kopp, et al., 2000). Although, seismic interpretation can resolve majority of tectonic structures, but due to resolution issues few small-scale and deeper structures need proper identification via attributes and velocity analysis techniques.

2.2.1 Subducting plate structures

The seismic profile covers a significant portion of the seafloor south of the deformational front, known as the Oman abyssal plain, which is located near the northern end of the Arabian microplate. The Little

Murry Ridge, Makran sands and Himalayan (Makran) turbidities are the part of the subducting plate (Kopp et al., 2000, Figure 2b). The Little Murray Ridge that cuts the seabed (Figure 2c) is not exposed on the sea floor in CAM-30 profile (Figure 2b) due to 5 km offset in the southern part of profiles. The most pronounced greatly disturbed bathymetric high as verified by interpreted seismic section (oceanic crust, Figure 2b) is identified at a depth of 8 km dipping northward along with Makran turbidities (Minshull et al., 1992). Above this the decollement lies within the Makran turbidities that dips shallow to nearly horizontal northward along the oceanic crust (Minshull et al., 1992; Fruehn et al., 1997; Kopp et al., 2000; Figure 2b). The entire belt is slipping northward along the weak decollement and faults generally got younger southwards (Ahmed, 1969; Farah et al., 1984). A very prominent unconformity known as Makran unconformity is marked on the top of Himalayan turbidities where Makran sands onlap southwards (Unconformity, Figure 2b).

A Trench is one of the primary structures of the subducting plate. In Makran, there is no morphological feature of a deep-sea trench along with active convergent margin. The high rate of sedimentation and low dip angle of the subducting plate means that no evidence of trench can be observed on seismic profile, but it can be marked in the frontal region of the deformational front (Priestley et al., 2022, Figure 2a, b). According to Fruehn et al. (1997), there is a 7 km thick sedimentary sequence south of the deformational boundary and sediments up to 3 km thick are subducting beneath the overriding sequence of imbricate thrusts, causing seismicity to become more dispersed and complex. Sediment accretion has been believed to start since 30-90 Myr in the MAW (White and Ross, 1979; Byrne et al., 1992; Dolati, 2010; Ball et al., 2019). Furthermore, to the south of the deformational front (~14 km), a newly uplifted sea floor area with potential thrusting is identified (Schluter et al., 2002, Figure 2b). This demonstrates stress localization/accumulation in a region and also deformational stages of the MAW. The newly emerging fault propagation fold is clearly seen at shallow depths (Fruehn et al., 1997; Figure 2b). The

entire rising on the seafloor known as the growing fold area is ~ 233 m due to successive slip on frontal ramp.

In the Oman basin, there exist highly fractured subducting plate sedimentary strata (White and Ross, 1979). A detailed study of these rocks (Himalayan turbidities) by seismic attribute analysis argues that the nature of the small-scale faulting/fracturing (Chambers and Yarus, 2002; Subrahmanyam and Rao, 2008; Koson et al., 2013) is related to the Little Murray Ridge or the flexure bulging (Christensen and Ruff, 1988; Masson, 1991; Ruiz and Contreras-Reyes, 2015). By the application of instantaneous dip, dip variance, parallel bed indicator, chaotic, and trace envelope attributes, the digital seismic data is decomposed into its different components (Subrahmanyam and Rao, 2008; Gogoi and Ghosh,2017). Instantaneous dip attributes are calculated sample by sample and provide a continuous change in attributes along the time and space axes. The variance property has been shown to be highly successful in helping to image channels, faults, and fracture zones (Pigott et al., 2013; Gogoi and Ghosh, 2017). Similarly, horizontal continuity and discontinuity is calculated by semblance and variance, where bedding dips give depositional information of the area (Subrahmanyam and Rao, 2008). The Chaos attribute depicts chaotic variances in dip and azimuth, which can effectively show reflector disruption spots. The maximum chaotic zones indicate discontinuities of reflectors such as fault and fracture zones (Pigott et al., 2013; Koson et al., 2013; Gogoi and Ghosh, 2017). The trace envelope attribute is directly related to the contrast of acoustic impedance/reflection strength, used for porosity variation and bright spots analysis (Taner, 2001). Additionally, similar attributes have been extracted from seismic data set dealing with depositional and structural behavior of clastic rocks in the South China sea (Pigott et al., 2013).

For small scale tectonic structures, we used seismic geometrical attributes such as instantaneous dip, parallel bedding indicator, chaotic and variance (Figure 3), and seismic physical attributes such as trace envelope to evaluate porous zones (Figure 4). Several authors argued that the Makran sands have high

porosity with possible fluid saturation (White, 1979; Minshull and White, 1989; Minshull et al., 1992). Furthermore, frontal area has high fluid pressure zones as conformed by the presence of mud volcanoes (Ellouz et al., 2007). The frequency of these mud volcanoes is considerably increased eastward with closely spaced cluster as compared to the western segment of MSZ, which might be attributed to an increase in eastward convergence rate (Kassi et al., 2014). The geometrical attributes indicate that the turbidities are fractured (Figure 3), while trace envelope attributes show that it is highly porous as well (Figure 4). This illustrates the high porous sand with possible high fluid pressure significantly decreasing the frictional properties (Zhang et al., 1990; Rutter and Glover, 2012), and strength of the medium directly affecting the deformation pattern of subduction megathrust and its structural style.

The velocity structure analysis was also carried out to support seismic interpretation (Figure 5). We utilized data from a wide-angle seismic reflection survey SO123 MAMUT (MAkran Murray Ridge Traverse) for velocity and regional structural study of the crust and upper mantle. For wide angle analysis, several sets of Ocean Bottom Seismometers (OBS) and Ocean Bottom Hydrophones (OBH) are deployed across the offshore frontal region of wedge. As indicated in Figure 2c, a total of 19 recoding instruments were installed along the SO 123-08 profile. The velocity model (Figure 5) has imaged the sedimentary layer as well as the subducting oceanic crust, indicating that the lateral velocity variations are not sharp and have lateral continuity. We have compared these offshore velocities with onshore shear wave velocities (Penney et al., 2017) and found that shear velocities change from 2.5-3.5 km/sec at the plate interface in offshore region as compared to 3.2-4.2 km/sec in the onshore region. This increase in seismic velocities towards onshore suggested a reduction in porosity (Fowler et al., 1985; Minshull and White, 1989).

2.3 Limit analysis approach

We adopt the limit analysis technique (Salencon, 2002; Chandrasekharaiah and Debnath, 2014), which is based on the principle of virtual powers and the maximum rock strength theorem (Maillot and Leroy, 2006). The Coulomb's criterion is used to describe maximum rock strength in this study. The virtual power principle consists of creating a virtual displacement across the accretionary wedge to study the distribution of faults under different tectonic settings (Maillot and Leroy, 2006; Salencon.,1972,1974; Cubas et al., 2008). This approach investigates the mechanical characteristics of the imbricate thrust fault system and optimizes them with an upper bound in relation to tectonic forces (Salencon.,1972,1974; Maillot and Leroy, 2006; Cubas et al., 2008). This technique has been widely used in literature to study the frictional characteristics of faults inside the accretionary wedge (Cubas et al., 2008, Cubas et al., 2013a, 2013b; Pons et al., 2013; Kuncoro et al., 2015).

Note that we assume a cohesion-less wedge for the limit analysis. To determine the position of active faults, we first setup the structure's frictional parameters: friction of sedimentary accretionary wedge or bulk ($\mu_{bulk} = \tan(\varphi_{bulk})$), and plate interface (PI) friction i.e., ($\mu_{PI} = \tan(\varphi_{PI})$), which may be frontal interface or back interface (Figure 6). For simulations, we use the commercial software Optum-G2-2020 in this work. Due to the fact that the Optum-G2 software does not handle over-pressure, we used effective frictions, which are defined as:

$$\mu = \tan(\varphi), \tag{1}$$

$$\mu_{eff} = \mu(1 - \lambda), \tag{2}$$

$$\tau = \mu(1 - \lambda)\sigma_z \tag{3}$$

In Equations (1-3), the τ, σ_z, μ, μ_{eff} and λ are the shear stress, normal stress, friction coefficient, effective friction coefficient and pore fluid pressure ratio for an accretionary wedge described by Davis et al. (1983).

$$\lambda = (P + \rho_w g D) / (|\sigma_z| + \rho_w g D) \quad (4)$$

In Equation (4), the P, D, σ_z, ρ_w and g are the pore fluid pressure, water depth, stress normal to the decollement, water density and gravity acceleration, respectively. We start with a simple geometry based on the interpreted CAM 30 profile to understand the mechanical requirements for the development of these structures. We utilize a ~120 km long section to depict the profile's frontal portion, which is formed by a triangular wedge (Figure 6).

We assume $\lambda = 0.4 - 0.6$ based on calculations by different authors for Makran region (Kukowski et al., 2001; smith et al., 2012; Wang and Hu, 2006; Pajang et al., 2021). Similarly, the velocity structure study has revealed that there is relatively slight variation in velocities within sedimentary strata (Figure 5). Based on these findings, we determined that the characteristics of the sedimentary strata are uniform. For the bulk properties of wedge, we choose an average friction for $\varphi_{bulk} = 30^{\circ}$; $\mu_{bulk} = 0.57$ (Byerlee, 1978), resulting in an effective friction of $\mu_{eff\_bulk} = 0.34$ (i.e., $\lambda_{bulk} = 0.4$) using Equations (1-2). As the MAW is composed of continental sediments comprising of siltstone, siltstone with shale, sandstone and shale (Pajang et al., 2021). For sensitivity analysis, we change the friction values from 0.5 to 0.64 in order to incorporate the 1-sigma uncertainty due to the presence of different lithologies. There is no significance effect of varying bulk friction in our results.

3. Results

We examine the 2D failure mode, in a profile through accretionary prism which describes ongoing thrusting in complicated fold belt areas of wedge. As a result, the mechanical conditions required to trigger a decollement and an imbricate sequential thrust system are being studied. According to the structural interpretation of seismic data (Figure 2), the area is characterized by an upward closely spaced southwards forethrust splay fault system. The purpose of this study is to identify the frictional characteristics that are important to replicate these findings. The study also investigates the effect of

altering the parameters based on material strength and structural geometry on the failure mechanism in accretionary wedges.

3.1 Faults generation due to frictional variation

Differential frictional values are leading the segmentation of the decollement due to mean normal stress changes and changes in effective frictions. Here, we performed several simulations using a planar subduction megathrust to get a better understanding of the model predictions. We select an initial geometry that keeps the wedge stable under critical condition in horizontal compression. Megathrust activation during simulation causes splay faults to form at the transition between distinct segments with differing friction strengths. There are two possibilities of splay faults either forethrust or backthrust depending on the friction properties. At the friction transition, a backthrust develops as friction values grow towards the foreland (trench), but a forethrust develops as friction decreases (Figure 7). The deformational structure of MAW has seaward verging imbricate thrust faults (Smith et al., 2012). The numerical technique is initially applied to a precisely 2D triangular wedge (Figure 6). The development of a splay fault, its corresponding backthrust, and partial or total activation of the decollement characterize the failure mechanism because of the applied force. For different values of the friction angle, the failure mechanism is characterized by thrust roots at the base of the back wall and the absence of back thrust (Pons and Leroy, 2012).

Figure 7 shows a single transition zone that split the interface into two segments having different frictional properties i.e., where $\mu_{eff\_PI\_bulk} > \mu_{eff\_PI\_front}$ (i.e., Case-I). While in case-II, the continuous subduction produces accretion and increases the normal stress field as compared to shear stress (tectonic stress), which can cause locking of the older fault (F1) and creating a new fault (F2). So, towards foreland further splitting into more segments can be observed. In case-III, the third splay fault (F3) generates and split the basal decollement into four segments allowing differential frictional properties and so on. The

continuous decrease in friction properties produces a sequence of forethrust splay fault system similar to MSZ across the MAW (Figure 2b).

3.2 Decollement and imbricated splay faults analysis

We first examine how to create a ramp as a splay fault along the plate interface (megathrust) that may or may not cut the surface topography (Figure 8). The selected wedge interface is subdivided into frontal interface and back interface. The maximum friction determined from numerical modeling for allowing slip along the plate interface is $\mu_{eff\_PI\_bulk} \leq 0.12$ (Table 1). For ramp development as a splay fault requires geometrical or frictional change along the plate interface (Kuncoro et al., 2015).

According to Georgiannopoulos and Brown (1978), Curran and Carroll (1979), Elliott and Brown (1986), Brown and Yu (1988) and Carroll (1991), the critical state theory can describe the deformation of porous sandstones as these are often weak and weakly cohesive. Porosity and the amount of effective mean stress have great impact on the strength and mode of inelastic failure. Lower-porosity rocks have greater ultimate strength than higher-porosity rocks and ultimate strength rises as mean stress rises (Zhang et al., 1990; Rutter and Glover, 2012). For a given porosity, the finer the grain size of a rock body, the greater the strength and vice versa (Zhang et al., 1990) and Makran sand have high porosity with possible fluid saturation (White, 1979; Minshull and White, 1989; Minshull et al., 1992).

We performed seismic attribute analysis based on digital seismic data i.e., for fracture zones analyses. The geometrical attributes analyses (Figure 3) indicate that the Makran turbidities are highly fractured, while trace envelope attributes (Figure 4) reveal Makran turbidities have high porosity.

3.3 The frontal wedge friction analysis

The interpretation of seismic data and seismicity of region showed that the deformational front and the newly uplifted region appear to be active. We can estimate its frictional characteristics, if any of the splay

fault or the plate interface is triggered co-seismically or by aseismic slip (Cubas et al., 2013b). Rice (2006) found that a high basal friction indicates aseismic fault slips, but a low effective friction might be caused by a long-term high pore pressure or dynamic weakening during co-seismic slip. Using the real geometry to study the frontal part of the profile, different scenarios for fault activation or new fault generation are as follows:

- Subduction interface can be activated
- Subduction interface is activated along with splay fault (F1).
- Subduction interface is activated along F1 and F2 splay faults.

To estimate maximum effective friction along major or its splay faults, several simulations are run with different friction values and then the outcomes are analyzed for deformation response. Different scenarios are represented in Table 1. The initial required condition for a plate interface to be activated with an effective friction must be equal or less than 0.12. If effective friction values exceed this, there will be no fault rupture along the megathrust. After the activation of the plate interface, distinct friction values are applied to analyze different deformation response of wedge (Table 1). The imbricate fault system is determined along with its deformation pattern at upper bounds condition. In scenario 2, the effective friction value at the plate back interface ($\mu_{eff} = 0.12$) is less than the frontal interface ($\mu_{eff} = 0.12, 0.13,$ and 0.14), the result is a backthrust. To recreate the imbricate fault system, we observed that friction values along the plate interface must be reduced by at least 25%. For example, in scenario 3 of Table 1, we observed forethrust deformation (Figure 7), when the frontal interface effective friction values ($\mu_{eff} = 0.09, 0.07,$ and 0.04) decreases than back interface ($\mu_{eff} = 0.12$). If the reduction rate of frontal segment friction values is <20%, there will be no proper development of fault (scenario 4, Table 1). Furthermore, when reduction rate of friction is too high, it can cause normal faulting as in scenario 5.

3.4 Frontal faults activation and slip assessment

The limit analysis approach is used to obtain virtual velocities for various blocks and discontinuities (i.e., faults). The ratio of virtual velocities of two blocks (after projection along their faults) is assumed to be equal to the ratio of displacement between the blocks (Cubas et al., 2013a, b). This permits us to assess the ratio of accommodated slip by each fault along the plate interface. According to Byrne et al. (1992), DeMets et al. (1994), Kopp et al. (2000), Smith et al. (2012), and Ball et al (2019), the convergence rate is 3-4 cm/yr and the large earthquakes along three patches of the eastern Makran offshore occurred in 1945, 1864 and 1765. We may expect 2.31-3.08 m, 4.74-6.32 m, and 7.71-10.28 m of slip for each patch along the plate interface at the back of the model, if these segments are completely locked and the frontal structures are only activated during earthquakes.

According to the mechanical modeling, if we rupture frontal plate interface and splay faults as shown in Figure 8, we could expect a range of slip i.e., 5.15 ± 2.47 m to 5.81 ± 2.78 m in horizontal direction and 0.69 ± 0.37 m to 3.02 ± 1.45 m in vertical direction due to 2.31-3.08 m, 4.74-6.32 m, and 7.71-10.28 m slip deficit along each patch. Such displacements can occur either along megathrust (low angle), its splay faults (high angle) or both. In addition, we showed that the splay faults have high uplift as compared to the plate interface. This would amplify the uplift of thick water column (~3000 m) and can generate a large tsunami in the coastal areas.

4. Discussion

The MSZ is poorly understood, yet potentially the largest source of earthquakes and tsunami hazards in the southern Pakistan. The increasing convergence rates between the Arabia and the Eurasia moving from west to east across the subduction zone initiates the slip partitioning into the megathrust motion. This differential convergence divides the MSZ into eastern and western parts with high and low seismicity, respectively (Kukowski et al., 2000). The Makran offshore has been struck by a tsunamigenic

M8.1 earthquake in 1945 (Pararas-Carayannis, 2006; Heidarzadeh et al., 2008), and it possess the potential to generate 8.7–9.2 (M_w) earthquakes (Smith et al., 2013; Frohling and Szeliga, 2016). Furthermore, splay faults play a vital role in understanding tsunamis and associated natural hazards over the coastal region of Pakistan. Splay faults are more susceptible to rupture and could accommodate large vertical displacement due to their steeper dip as compared to the megathrust. According to Willett (1992), variation in geometry, strength or size of wedge are linked to deformation pattern, which are analyzed by frictional properties at plate interface.

The digital seismic profiles are interpreted to investigate different tectonic structures i.e., the megathrust and associated splay faults as an imbricate fault system with landwards dipping thrust (Figure 2b). The faults extend up to the surface except for the newly emerging fault propagating fold (Ahmed, 1969; Raza et al., 1981; Farah et al., 1984; Fruehn et al., 1997; Kopp et al., 2000). The concentration of deformation (uplifting at seafloor ~233 m) at newly frontal fault region of MAW indicates the decrease in decollement strength (Willett, 1992). Similarly, seismic data evidently shows the geological structures of the subducting plate i.e., flexure bulging, Little Murray Ridge, Makran turbidities and Makran sands.

Mechanical modeling illustrates the formation of tectonic structures and related friction properties (Figures 7, 8). For structural analysis, an effective friction ≤ 0.12 is required to trigger the decollement to reproduce the observed geometry of MAW. The model shows the effect of friction properties along the megathrust and its response (Figure 7). For example, backthrust system of faults are common in area where frontal section has relatively higher friction values, while forethrust system are formed in the areas where we observed low values of friction in frontal section. There may be two reasons to the low effective frictions, 1) due to high pore pressure or 2) dynamic weakening mechanism (Kuncoro et al., 2015). Furthermore, the low friction on the subduction megathrust is indicated by several parameters; 1) presence of mud volcano onshore and variation in heat flow (Ferguson, 1990), and 2) the low decollement and surface dips can cause high pore pressure (Davis et al., 1983). The effective friction is estimated

approximately 0.04-0.12 for the eastern Makran indicating low friction values at the frontal interface of MAW, consistent with the other studies about eastern Makran (Kukowski et al., 2001: μ_{eff} ~0.152 ; Smith et al., 2012: μ_{eff} ~ 0.04- 0.18 ; Penny et al., 2017: μ_{eff} ~0.01-0.03) and other subduction zones (Von Herzen et al ., 2001 $\mu_{eff} < 0.1$ for Kermadec forearc ; Lamb, 2006 : μ_{eff} ~ 0.025-0.12; Kuncoro et al., 2015: μ_{eff} ~ 0.035-0.12 for southern Sumatra subduction zone). The effective friction values decrease significantly if pore pressure of wedge exceeds the hydrostatic pressure (Kuncoro et al., 2015). For example, Davis et al. (1983) and Lamb (2006) estimated effective friction <0.03 for λ >0.90. Therefore, Cubas et al. (2013a) illustrated that forethrust imbricate fault system are the result of low friction values on main decollement.

Our analysis suggests that low friction properties in the frontal area are one of major reason of landward dipping imbricate system in MSZ (Figure 8). In MSZ, mud volcano eruptions, mudslides, and liquefaction are the most common during or absence of seismic shaking (Rajendran et al., 2013). The presence of mud volcanoes indicates high pore-fluid pressure region (White, 1979; Minshull and White, 1989; Delisle et al., 2002; Schluter et al., 2002; Ellouz et al., 2007), causing decrease in friction properties of frontal Makran wedge. Willett (1992) stated that the deformation concentration at the toe of the wedge is the result of decrease in the strength of decollement. Furthermore, Zhang et al. (1990) revealed strength of rock decreases for a given porosity of coarser grain size and increases for smaller grain size. This increase in porosity reduce the strength of the rock having significant impact on the frictional properties of the decollement and its splays fault formation (Georgiannopoulos and Brown, 1978; Curran and Carroll, 1979; Elliott and Brown, 1986; Brown and Yu, 1988; Carroll, 1991).

The slip accumulation since 1945, 1864 and 1765 earthquakes along each patch of eastern MSZ is 2.31-3.08 m, 4.74-6.32 m, and 7.71-10.28 m, respectively. This implies that the area possesses large tsunamigenic potential. From the modeling, if the frontal faults i.e., splays or megathrust are re-activated,

we expect differential slip along each fault. For example, if the splay faults (F1, F2) are activated with interface (Figure 8), the range of horizontal and vertical slip components are 5.15 ± 2.47 m to 5.81 ± 2.78 m and 0.69 ± 0.37 m to 3.02 ± 1.45 m, respectively. The variation in vertical component of the slip is higher as compared to the horizontal component of slip along each fault. This highlights that the splay faults possess more uplift due to its high dip angle as compared to low angle megathrust and are more susceptible to generate near field devastating tsunami.

In accretionary wedges, subduction megathrust are connected to splay faults that propagate with the deposition of sediments from overriding plate (Sykes and Menke, 2006). Wang and Hu (2006) indicated that the frontal region of the wedge is more susceptible to accommodating elastic strain in its stable part due to weak material and therefore it aggressively contributes in the splay faults rupture. Fukao (1979) proposed that splay fault rupture propagation is one of the key sources to generate devastating tsunamis. Many great subduction earthquakes, such as the 1944, 1946, 1960, 1964, and 2004 Tonankai, Nankai, Chili, Alaska, and Sumatra respectively, have shown that splay faults assisted in tsunami generation (Cummins and Kaneda, 2000; Heidarzadeh, 2011). Out of these great earthquakes, only the 2004 Sumatra tsunami (Geist et al., 2006) killing around 225,000 people has properly highlighted the importance to study earthquake and tsunami threats for various vulnerable coasts throughout the world, particularly those bordering the Indian Ocean.

Based on available seismological data, most of tsunamigenic potential earthquakes occurred at shallow depth i.e., <20 km (Jackson and McKenzie, 1984; Satake and Tanioka, 1999). According to Heidarzadeh et al. (2008) and Burg (2018), the offshore area of the Makran demonstrate shallow seismicity with a depth range up to 20 km. The whole area of the Makran is vulnerable for tsunami potential due to subduction megathrust and its splay faults. Makran splay faults, in comparison to the subduction megathrust possess a higher risk of large earthquakes, which can generate a disastrous tsunami in nearby areas like Gwadar, Pasni, Ormara, Somiani and Karachi.

5. Conclusions

Coastal regions across the world are at high risk of earthquakes and tsunamis due to continuous deformation at subduction zones. Understanding the deformation processes and associated seismic potential risks require knowledge of mechanical properties (i.e., friction properties, pore pressure etc.,). Here, we investigate the importance of mechanical characteristics within the context of deformation style of the MSZ. The digital seismic profiles passing near to the location of 1945 tsunamigenic event (the second worst tsunami in the Indian Ocean after 2004 Sumatra tsunami) are used to characterize the wedge. The investigated eastern part of world largest MAW consists of splay faults both onshore and offshore with seaward verging thrusts. The seismic attributes are applied to investigate the factors controlling the friction strength of strata. We observed that the frontal portion of the MSZ is fractured under high pore pressures, that lowers the strata's friction values implying a reduction in decollement strength.

The tectonic slip accumulation by considering both earthquake gap and rate of convergence along the MSZ are studied and used for fault slip analysis. This estimates the displaced slip components of future earthquake rupture. From mechanical modeling, the effective friction values must be ≤ 0.12 to activate the plate interface. We observed that the region has low friction values at the frontal interface that may be due to high pore pressure or dynamic weakening. The ongoing subduction after the 1945, 1864 and 1765 large earthquakes can produce considerable deformation i.e., 2.31-3.08 m, 4.74-6.32 m, and 7.71-10.28 m, if the frontal region is locked. Instead of whole wedge displacement, reactivating frontal splay faults would result in horizontal displacement and vertical uplift ranging from 5.15 ± 2.47 m to 5.81 ± 2.78 m and 0.69 ± 0.37 m to 3.02 ± 1.45 m, respectively. As a result, the region is at high risk of a large earthquake followed by a significant tsunami.

Acknowledgements

The authors would like to acknowledge both the Department of Earth Sciences, Quaid-i-Azam University, Islamabad, and the Center for Earthquake Studies (CES), National Center for Physics (NCP), Islamabad, Pakistan, for their support. We thank Professor Tim Minshull, School of Ocean and Earth Science, University of Southampton, National Oceanography Centre Southampton, European Way Southampton SO14 3ZHUK for providing high-resolution seismic reflection data for research. We are thankful to the OPTUM G2 team for permitting us an academic license of the software Optum-G2 2020 for completing this research work. The authors would also like to thank Dr. Khurram Shehzad Aslam, Department of Earth Sciences, University of Oregon, USA (Geoscientist) for reviewing this manuscript carefully for English structure, grammar, and style.

Author statements

Mr. Shaukat Parvaiz perceived the idea and partially executed this idea of the research as well as his contribution in terms of collection of the literature and raw data. Dr. Aamir Ali took the idea and proposed the methodology and implemented along with interpretation and finalization of the manuscript. Dr. Farhan Javed have given the support in terms of modern research methods and helped in the interpretation of the data. Muhammad Ali Shah has given the data support and generated the maps.

References

Abedi, M., Bahroudi, A., 2016. A geophysical potentialfield study to image the Makran subduction zone in SE of Iran. Tectonophysics 688, 119–134.

Ahmed, S.S., 1969. Tertiary geology of part of south Makran, Baluchistan, West Pakistan. AAPG lletin, 53(7), 1480-149.

Aslam, K.S., Thomas, A.M., Melgar, D., 2021. The Effect of Fore-Arc Deformation on Shallow Earthquake Rupture Behavior in the Cascadia Subduction Zone. Geophysical Research Letters, 48 (20), e2021GL093941.

Ball, T.V., Penney, C.E., Neufeld, J.A., Copley, A.C., 2019. Controls on the geometry and evolution of thin-skinned fold-thrust belts, and applications to the Makran accretionary prism and Indo–Burman Ranges. Geophysical Journal International, 218(1), 247-267.

Ambraseys, N.N., Melville, C.P., 2005. A history of Persian earthquakes. Cambridge university press.

Bonnardot, M.A., Hassani, R., Tric, E., Ruellan, E., Régnier, M., 2008. Effect of margin curvature on plate deformation in a 3-D numerical model of subduction zones. Geophysical Journal International, 173 (3), 1084-1094.

Brown, E.T., Yu, H.S., 1988. A model for the ductile yield of porous rock. International Journal for Numerical and Analytical Methods in Geomechanics, 12 (6), 679-688.

Burg, J.P., 2018. Geology of the onshore Makran accretionary wedge: Synthesis and tectonic interpretation. Earth-Science Reviews, 185, 1210-1231.

Byerlee, J., 1978. Friction of rocks: Pure and Applied Geophysics. 116, 615-626.

Byrne, D.E., Davis, D.M., Sykes, L.R., 1988. Loci and maximum size of thrust earthquakes and the mechanics of the shallow region of subduction zones. Tectonics, 7 (4), 833-857.

Byrne, D.E., Sykes, L.R., Davis, D.M., 1992. Great thrust earthquakes and aseismic slip along the plate boundary of the Makran subduction zone. Journal of Geophysical Research: Solid Earth, 97 (B1), 449-478.

Carroll, M.M., 1991. A critical state plasticity theory for porous reservoir rock. Recent advances in mechanics of structured continua, 117, 1-8.

Chandrasekharaiah, D.S., Debnath, L., 2014. Continuum mechanics. Elsevier.

Chambers, R.L., Yarus, J.M., 2002. Quantitative use of seismic attributes for reservoir characterization. CSEG recorder, 27 (6), 14-25.

Chapple, W.M., 1978. Mechanics of thin-skinned fold-and-thrust belts. Geological Society of America Bulletin, 89 (8), 1189-1198.

Chopra, S., Marfurt, K.J., 2005. Seismic attributes—A historical perspective. Geophysics, 70 (5), 3SO-28SO.

Chopra, S., Marfurt, K., 2006. Seismic Attributes–a promising aid for geologic prediction. CSEG Recorder, 31,110-120.

Christensen, D.H., Ruff, L.J., 1988. Seismic coupling and outer rise earthquakes. Journal of Geophysical Research: Solid Earth, 93 (B11), 13421-13444.

Cubas, N., Y. M. Leroy., B. Maillot., 2008. Prediction of thrusting sequences in accretionary wedges, Journal of Geophysical Research, 113 (B12), 1–21.

Cubas, N., Avouac, J.P., Souloumiac, P., Leroy, Y., 2013a. Megathrust friction determined from mechanical analysis of the forearc in the Maule earthquake area. Earth and Planetary Science Letters, 381, 92-103.

Cubas, N., Avouac, J.P., Leroy, Y.M., Pons, A., 2013b. Low friction along the high slip patch of the 2011 Mw 9.0 Tohoku-Oki earthquake required from the wedge structure and extensional splay faults. Geophysical Research Letters, 40 (16), 4231-4237.

Cubas, N., Barnes, C., Maillot, B., 2013c. Inverse method applied to a sand wedge: estimation of friction parameters and uncertainty analysis. Journal of Structural Geology, 55, 101-113.

Curran, J.H., Carroll, M.M., 1979. Shear stress enhancement of void compaction. Journal of Geophysical Research: Solid Earth, 84 (B3), 1105-1112.

Cummins, P.R., Kaneda, Y., 2000. Possible splay fault slip during the 1946 Nankai earthquake. Geophysical Research Letters, 27 (17), 2725-2728.

Dahlen, F.A., Suppe, J., Davis, D., 1984. Mechanics of fold-and-thrust belts and accretionary wedges: Cohesive Coulomb theory. Journal of Geophysical Research: Solid Earth, 89 (B12), 10087-10101.

Davis, D.M., 1978. The mechanics of thrust faults: a sandbox model. BS: Princeton University, Princeton, NJ.

Davis, D.M., Suppe, J., 1980. Critical taper in mechanics of fold-and-thrust belts. In Geological society of America Abstract Programs, 12, 410.

Davis, D., Suppe, J., Dahlen, F.A., 1983. Mechanics of fold-and-thrust belts and accretionary wedges. Journal of Geophysical Research: Solid Earth, 88 (B2), 1153-1172.

Delisle, G., Von Rad, U., Andruleit, H., Von Daniels, C., Tabrez, A., Inam, A., 2002. Active mud volcanoes on-and offshore eastern Makran, Pakistan. International Journal of Earth Sciences, 91(1), 93-110.

DeMets, C., Gordon, R.G., Argus, D.F., Stein, S., 1994. Effect of recent revisions to the geomagnetic reversal time scale on estimates of current plate motions. Geophysical research letters, 21 (20), 2191-2194.

Dolati, A., 2010. Stratigraphy, structural geology and low-temperature thermochronology across the Makran accretionary wedge in Iran, PhD thesis, Swiss Institute of Technology Zurich.

Elliott, G.M., Brown, E.T., 1986. Further development of a plasticity approach to yield in porous rock. In International Journal of Rock Mechanics and Mining Sciences & Geomechanics Abstracts, 23, No. 2, 151-156.

Ellouz-Zimmermann, N., Lallemant, S.J., Castilla, R., Mouchot, N., Leturmy, P., Battani, A., Buret, C., Cherel, L., Desaubliaux, G., Deville, E., Ferrand, J., 2007. Offshore frontal part of the Makran Accretionary prism: The Chamak survey (Pakistan). In Thrust belts and foreland basins, 351-366.

Farah, A., Abbas, G., De Jong, K.A., Lawrence, R.D., 1984. Evolution of the lithosphere in Pakistan. Tectonophysics, 105 (1-4), 207-227.

Ferguson, I.J., 1990. Numerical modeling of heat flow and fluid flow in subduction-accretion complexes. PhD Thesis. University of Birmingham.

Flueh, E.R., Kukowski, N., Reichert, C., 1997. FS Sonne Cruise Report SO123, Makran-Murray Traverse. GEOMAR Report ISSN. 0936-5788.

Fowler, S.R., White, R.S., Louden, K.E., 1985. Sediment dewatering in the Makran accretionary prism. Earth and Planetary Science Letters, 75 (4), 427-438.

Frohling, E., Szeliga, W., 2016. GPS constraints on interplate locking within the Makran subduction zone. Geophysical Supplements to the Monthly Notices of the Royal Astronomical Society, 205 (1), 67-76.

Fruehn, J., White, R.S., Minshull, T.A., 1997. Internal deformation and compaction of the Makran accretionary wedge. Terra nova, 9 (3), 101-104.

Fukao, Y., 1979. Tsunami earthquakes and subduction processes near deep-sea trenches. Journal of Geophysical Research: Solid Earth, 84 (B5), 2303-2314.

Fuller, C.W., Willett, S.D., Brandon, M.T., 2006. Formation of forearc basins and their influence on subduction zone earthquakes. Geology, 34 (2), 65-68.

Geist, E.L., Titov, V.V., Synolakis, C.E., 2006. Tsunami: wave of change. Scientific American, 294 (1), 56-63.

Gerogiannopoulos, N.G., Brown, E.T., 1978. The critical state concept applied to rock. In International Journal of Rock Mechanics and Mining Sciences & Geomechanics Abstracts, 15 (1), 1-10.

Gogoi, M., Ghosh, G.K., 2017. Interpretation of Seismic data for thrust/fault identification using variance and inverse of variance attribute analysis. J. Ind. Geophys, 21 (6), 500-506.

Harms, J.C., Cappel, H.N., Francis, D.C., 1984. The Makran coast of Pakistan: its stratigraphy and hydrocarbon potential. Marine geology and oceanography of Arabian Sea and coastal Pakistan, 3, 27.

Hassani, R., Jongmans, D., Chéry, J., 1997. Study of plate deformation and stress in subduction processes using two-dimensional numerical models. Journal of Geophysical Research: Solid Earth, 102 (B8), 17951-17965.

Heidarzadeh, M., Pirooz, M., Zaker, N., Synolakis, C., 2008. Evaluating Tsunami Hazard in the Makran Subduction zone off the southern coasts of Iran and Pakistan and results of numerical modeling. Ocean Engineering, 35, 774-786.

Heidarzadeh, M., 2011. Major tsunami risks from splay faulting. Environmental Sciences, 67-80.

Jackson, J., McKenzie, D., 1984. Active tectonics of the Alpine Himalayan Belt between western Turkey and Pakistan. Geophysical Journal International, 77 (1), 185-264.

Jacob, K.H., Quittmeyer, R.C., 1978. Makran Region of Pakistan and Iran-Trench-Arc System with Active Plate Subduction. Trans Am Geophys Union, 59 (4), 323-323.

Kassi, A.M., Khan, S.D., Bayraktar, H., Kasi, A.K., 2014. Newly discovered mud volcanoes in the Coastal Belt of Makran, Pakistan—tectonic implications. Arabian Journal of Geosciences, 7 (11), 4899-4909.

Kopp, C., Fruehn, J., Flueh, E.R., Reichert, C., Kukowski, N., Bialas, J., Klaeschen, D., 2000. Structure of the Makran subduction zone from wide-angle and reflection seismic data. Tectonophysics, 329 (1-4), 171-191.

Koson, S., Chenrai, P., Choowong, M., 2013. Seismic attributes and their applications in seismic geomorphology. Bulletin of Earth Sciences of Thailand, 6 (1), 1-9.

Kukowski, N., Schillhorn, T., Flueh, E.R., Huhn, K., 2000. Newly identified strike-slip plate boundary in the northeastern Arabian Sea. Geology, 28 (4), 355-358.

Kukowski, N., Schillhorn, T., Huhn, K., von Rad, U., Husen, S., Flueh, E.R., 2001. Morphotectonics and mechanics of the central Makran accretionary wedge off Pakistan. Marine Geology, 173 (1-4), 1-19.

Kuncoro, A.K., Cubas, N., Singh, S.C., Etchebes, M., Tapponnier, P., 2015. Tsunamigenic potential due to frontal rupturing in the Sumatra locked zone. Earth and Planetary Science Letters, 432, 311-322.

Laane, J.L., Chen, W.P., 1989. The Makran earthquake of 1983 April 18: A possible analogue to the Puget Sound earthquake of 1965?. Geophysical Journal International, 98 (1), 1-9.

Lallemand, S.E., Schnürle, P., Malavieille, J., 1994. Coulomb theory applied to accretionary and nonaccretionary wedges: Possible causes for tectonic erosion and/or frontal accretion. Journal of Geophysical Research: Solid Earth, 99 (B6), 12033-12055.

Lamb, S., Davis, P., 2003. Cenozoic climate change as a possible cause for the rise of the Andes. Nature, 425 (6960), 792-797.

Lehner, F.K., 1986. Comments on "Noncohesive critical Coulomb wedges: An exact solution". J. Geophys. Res. 9, 793–796.

Lamb, S., 2006. Shear stresses on megathrusts: Implications for mountain building behind subduction zones. Journal of Geophysical Research: Solid Earth, 111 (B7).

Lin, Y.N., Jolivet, R., Simons, M., Agram, P.S., Martens, H.R., Li, Z., Lodi, S.H., 2015. High interseismic coupling in the Eastern Makran (Pakistan) subduction zone. Earth and Planetary Science Letters, 420, 116-126.

Maggi, A., Jackson, J.A., Priestley, K., Baker, C., 2000. A re-assessment of focal depth distributions in southern Iran, the Tien Shan and northern India: Do earthquakes really occur in the continental mantle?. Geophysical Journal International, 143 (3), 629-661.

Maillot, B., Leroy, Y.M., 2006. Kink-fold onset and development based on the maximum strength theorem. Journal of the Mechanics and Physics of Solids, 54 (10), 2030-2059.

McNutt, M.K., Menard, H.W., 1982. Constraints on yield strength in the oceanic lithosphere derived from observations of flexure. Geophysical Journal International, 71 (2), 363-394.

Masson, D.G., 1991. Fault patterns at outer trench walls. Marine Geophysical Researches, 13 (3), 209-225.

Minshull, T., White, R., 1989. Sediment compaction and fluid migration in the Makran accretionary prism. Journal of Geophysical Research: Solid Earth, 94 (B6), 7387-7402.

Minshull, T.A., White, R.S., Barton, P.J., Collier, J.S., 1992. Deformation at plate boundaries around the Gulf of Oman. Marine Geology, 104 (1-4), 265-277.

Page, W.D., Alt, J.N., Cluff, L.S., Plafker, G., 1979. Evidence for the recurrence of large-magnitude earthquakes along the Makran coast of Iran and Pakistan. Tectonophysics, 52 (1-4), 533-547.

Pajang, S., Cubas, N., Letouzey, J., Le Pourhiet, L., Seyedali, S., Fournier, M., Agard, P., Khatib, M.M., Heyhat, M., Mokhtari, M., 2021. Seismic hazard of the western Makran subduction zone: insight from mechanical modelling and inferred frictional properties. Earth and Planetary Science Letters, 562, 116789.

Pararas-Carayannis, G., 2006. The potential of tsunami generation along the Makran Subduction Zone in the northern Arabian Sea: Case study: The earthquake and tsunami of November 28, 1945. Science of Tsunami Hazards, 24 (5), 358-384.

Park, J.O., Tsuru, T., Kodaira, S., Cummins, P.R., Kaneda, Y., 2002. Splay fault branching along the Nankai subduction zone. Science, 297 (5584), 1157-1160.

Penney, C., Tavakoli, F., Saadat, A., Nankali, H.R., Sedighi, M., Khorrami, F., Sobouti, F., Rafi, Z., Copley, A., Jackson, J., Priestley, K., 2017. Megathrust and accretionary wedge properties and behaviour in the Makran subduction zone. Geophysical Journal International, 209 (3), 1800-1830.

Pigott, J.D., Kang, M.H., Han, H.C., 2013. First order seismic attributes for clastic seismic facies interpretation: Examples from the East China Sea. Journal of Asian Earth Sciences, 66, 34-54.

Platt, J.P., Leggett, J.K., Young, J., Raza, H., Alam, S., 1985. Large-scale sediment underplating in the Makran accretionary prism, southwest Pakistan. Geology, 13 (7), 507-511.

Pons, A., Leroy, Y.M., 2012. Stability of accretionary wedges based on the maximum strength theorem for fluid-saturated porous media. Journal of the Mechanics and Physics of Solids, 60 (4), 643-664.

Pons, A., Leroy, Y.M., Lallemant, S., 2013. Fluid pressure control on splay fault activation in accretionary prism based on the maximum strength theorem with application to the Nankai wedge. Earth and Planetary Science Letters, 368, 43-50.

Priestley, K., Sobouti, F., Mokhtarzadeh, R., A Irandoust, M., Ghods, R., Motaghi, K., Ho, T., 2022. New Constraints for the On-Shore Makran Subduction Zone Crustal Structure. Journal of Geophysical Research: Solid Earth, 127 (1), p.e2021JB022942.

Quittmeyer, R.C., Jacob, K.H., 1979. Historical and modern seismicity of Pakistan, Afghanistan, northwestern India, and southeastern Iran. Bulletin of the Seismological Society of America, 69 (3), 773-823.

Rajendran, C.P., Rajendran, K., Shah-Hosseini, M., Beni, A.N., Nautiyal, C.M., Andrews, R., 2013. The hazard potential of the western segment of the Makran subduction zone, northern Arabian Sea. Natural hazards, 65 (1), 219-239.

Raza, H.A., Alam, S., Ali, S.M., Elahi, N., Anwar, M., 1981. Hydrocarbon potential of Makran region of Baluchistan basin. In Seminar on mineral policy of Baluchistan, Geo-logical Survey of Pakistan, Quetta.

Rice, J.R., 2006. Heating and weakening of faults during earthquake slip. Journal of Geophysical Research: Solid Earth, 111 (B5).

Ruff, L.J., Tichelaar, B.W., 1996. What controls the seismogenic plate interface in subduction zones?. Washington DC American Geophysical Union Geophysical Monograph Series, 96, 105-111.

Ruiz Paredes, J., Contreras Reyes, E., 2015. Outer rise seismicity boosted by the Maule 2010 Mw 8.8 megathrust earthquake. Tectonophysics 653, 127–139.

Rutter, E.H., Glover, C.T., 2012. The deformation of porous sandstones; are Byerlee friction and the critical state line equivalent?. Journal of Structural Geology, 44, 129-140.

Salençon, J., 1974. THEORIE DE LA PLASTICITE POUR LES APPLICATIONS A LA MECANIQUE DES SOLS.

Salençon, J., 2002. De l'élasto-plasticité au calcul à la rupture. Editions Ecole Polytechnique.

Satake, K., Tanioka, Y., 1999. Sources of tsunami and tsunamigenic earthquakes in subduction zones. Pure and Applied Geophysics, 154 (3), 467-483.

Scawthorn, C., Chen, W.F., 2002. Earthquake engineering handbook. CRC press.

Schlüter, H.U., Prexl, A., Gaedicke, C., Roeser, H., Reichert, C., Meyer, H., Von Daniels, C., 2002. The Makran accretionary wedge: sediment thicknesses and ages and the origin of mud volcanoes. Marine Geology, 185 (3-4), 219-232.

Smith, G., McNeill, L., Henstock, T.J., Bull, J., 2012. The structure and fault activity of the Makran accretionary prism. Journal of Geophysical Research: Solid Earth, 117 (B7).

Smith, G.L., McNeill, L.C., Wang, K., He, J., Henstock, T.J., 2013. Thermal structure and megathrust seismogenic potential of the Makran subduction zone. Geophysical Research Letters, 40 (8), 1528-1533.

Stockmal, G.S., Chapple, W.M., 1981. Modelling accretionary wedge deformation using a rigid-prefectly plastic rheology. Eos Transactions AGU, 62, 397-398.

Subrahmanyam, D., Rao, P.H., 2008. Seismic attributes-A review. In 7th international conference & exposition on petroleum geophysics, Hyderabad, 398-404.

Sykes, L.R., Menke, W., 2006. Repeat times of large earthquakes: Implications for earthquake mechanics and long-term prediction. Bulletin of the Seismological Society of America, 96 (5), 1569-1596.

Taner, M.T., Koehler, F., Sheriff, R.E., 1979. Complex seismic trace analysis. Geophysics, 44 (6), 1041-1063.

Taner, M.T., 2001. Seismic attributes. CSEG recorder, 26 (7), 48-56.

Wang, K., Hu, Y., 2006. Accretionary prisms in subduction earthquake cycles: The theory of dynamic Coulomb wedge. Journal of Geophysical Research: Solid Earth, 111 (B6).

White, R.S., Ross, D.A., 1979. Tectonics of the western Gulf of Oman. Journal of Geophysical Research: Solid Earth, 84 (B7), 3479-3489.

White, R.S., 1979. Deformation of Makran Continental Margin. In: Farah and Dejong, Eds., Geodynamics of Pakistan. Geological Survey of Pakistan, Quetta, 195-304.

White, R.S., 1982. Deformation of the Makran accretionary sediment prism in the Gulf of Oman (north-west Indian Ocean). Geological Society, London, Special Publications, 10 (1), 357-372.

White, R.S., Louden, K.E., 1982. The Makran continental margin: structure of a thickly sedimented convergent plate boundary: convergent margins: field investigations of margin structure and stratigraphy. 499–518.

Willett, S.D., 1992. Dynamic and kinematic growth and change of a Coulomb wedge. In Thrust tectonics, 19-31.

Zhang, J., Wong, T.F., Davis, D.M., 1990. Micromechanics of pressure-induced grain crushing in porous rocks. Journal of Geophysical Research: Solid Earth, 95 (B1), 341-352.

List of Figures along with captions

Figure 1: Seismo-tectonic map of study area. (a) Seismicity, with earthquake magnitude ≥ 3.0 shown as colored circles, for period of 1900 to recent. (b) The magnitude of earthquakes is symbolized with focal mechanism (Penney et al., 2017) and cyan color circles (Heidarzadeh, 2011; Local Catalogue). The tectonic features such as major boundaries and other associated faults are given as Makran Accretionary Wedge (MAW), Murray Ridge (MR), Makran Subduction Zone (MSZ), Ghazaband Fault (GF), Chaman Fault (CF), Siahan Fault (SiF), Panjgur Fault (PF), Pirandar Fault (PiF), Ornach Nal Fault (OF), Hab Fault (HF), Pab Fault (PF), Sonne Fault (SF), Minab Fault (MF), Oman Thrust (OT) and Zagros Thrust (ZT).

Figure 2: (a) CAM-30 uninterpreted depth section (b) Interpreted depth-migrated seismic reflection profile (Minshull et al., 1992; Kopp et al., 2000; Fruehn et al., 1997), with major subducting and overriding plates structures as marked with different colors, multiple (cyan), oceanic crust/Little Murray Ridge (golden), decollement (pink), Makran unconformity (yellow), water bottom reflector (green) and imbricate fault system (black) (c) Structural analysis from single channel profile SO 123-08 (https://oceanrep. geomar.de/id/eprint/27136/). Little Murray Ridge has an outcrop in Oman abyssal plane. Numbers at the top of seismic profile shows the location of ocean bottom hydrophone/seismometer.

Figure 3: Several attributes display for figure 2b; (a) Instantaneous dip shows high dip zone (maroon color) of forelimb side in the newly emerging fault propagating fold. (b) Parallel bed indicator highlights bedding continuity i.e., low values (blue color) indicate high coherence of traces while high values (brown color) show less coherence i.e., fracture zone. (c) Chaos depicts fracture/fault zones (light color) while low values (dark color) indicate less disturb zones (d) Variance better resolve the continuous reflectors as compared to disrupted zone.

Figure 4: Trace envelope attribute display for figure 2b, which demonstrates high values of amplitude/reflection strength (red color) pointed by black arrows both in Makran sands and turbidites.

Figure 5: P-waves structural analysis of profile SO 123-08. Velocity analysis was carried out on seven OBH/OBS positions and its interpolation to generate a velocity structure along the subduction area. The velocity structural thickness increases from left to right as oceanic crust subducts gently beneath the wedge as crossing OBS-5.

Figure 6: (a) Simple 2D-model set-up for geometrical analysis of the deformational front area of accretionary wedge and plate interface (PI). Friction along back, and front region of PI are as μ_{PI_back} and μ_{PI_front}. The $\mu_{\_bulk}$ show bulk friction values of the wedge material. (b) Model set-up for numerical simulation by mesh generation to study how to activate the megathrust at the plate interface and its response along the megathrust as well as the new splay faults (F1, F2 and F3) generation with change in the frictional properties. The topographic slope and plate interface dip are low and constant.

Figure 7: Forethrust generation of splay faults (i.e., F1, F2 and F3) due to decrease in basal effective friction towards the toe of wedge. The normalized virtual vertical velocity field shows the relative motion between the blocks in the vertical direction.

Figure 8: Normalized mean virtual velocity field for a) the generation of splay fault and b) minimal amount of slip expected for the scenario 3 (plate interface activated up to the trench).

List of Tables along with captions

Table-1. Values of effective frictions (μ_{eff}) at the plate back and front interfaces for the different five scenarios.

Table-2. Expected horizontal (δx) and vertical (δy) slip for scenario 3 along the plate interface (PI) and the two splay faults (F1 and F2) for three slip deficits applied at the back of the structure.

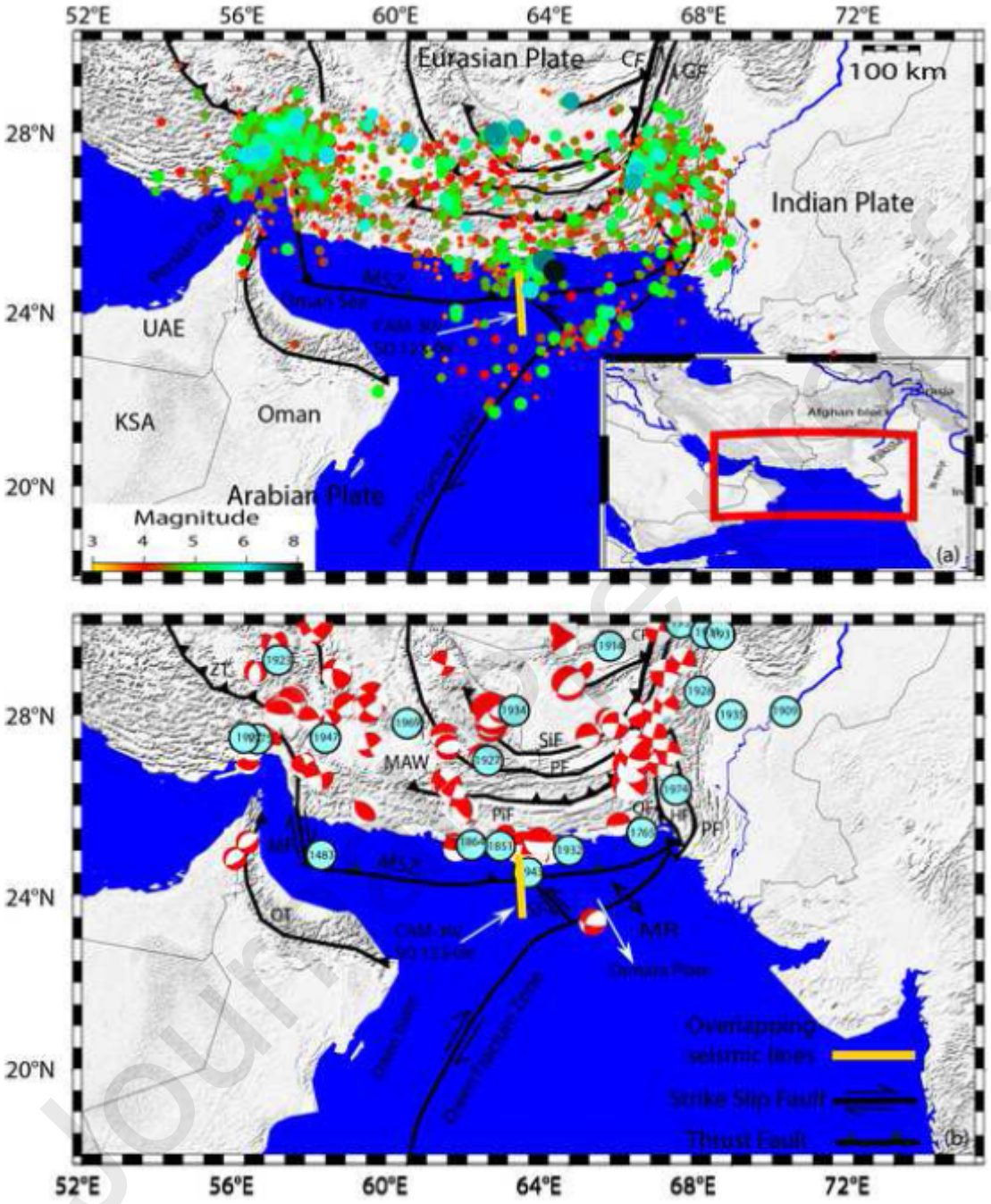
52°E
56°E
60°E
64°E
68°E
72°E
28°N
24°N
20°N
Eurasian Plate
CF
IGF
100 km
Indian Plate
UAE
KSA
Oman
Arabian Plate
Magnitude
3
4
5
6
8
(a)
ZT
MAW
SiF
PF
PiF
OF
HF
MR
OT
Overlapping seismic lines
Strike Slip Fault
Thrust Fault
(b)

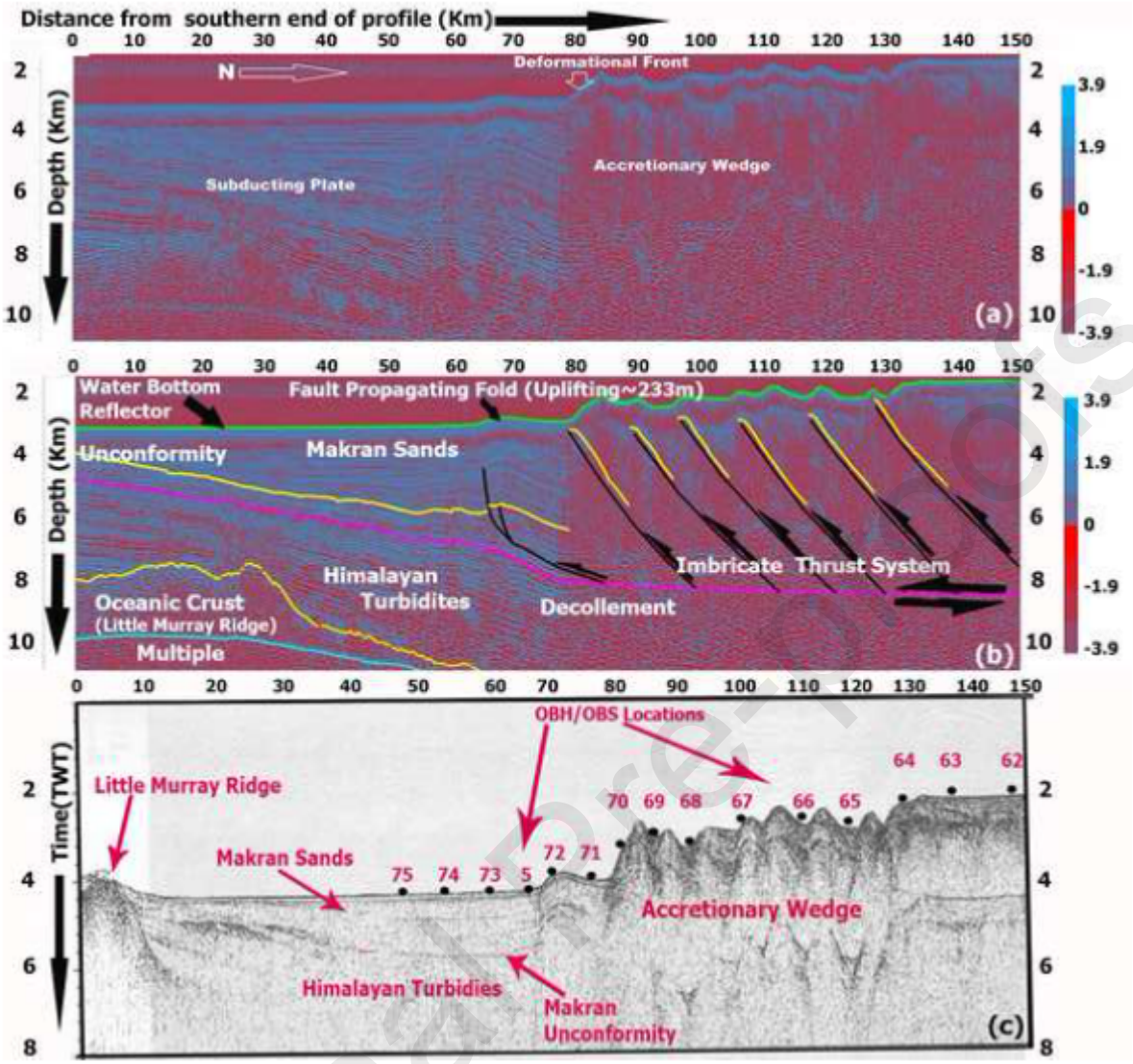

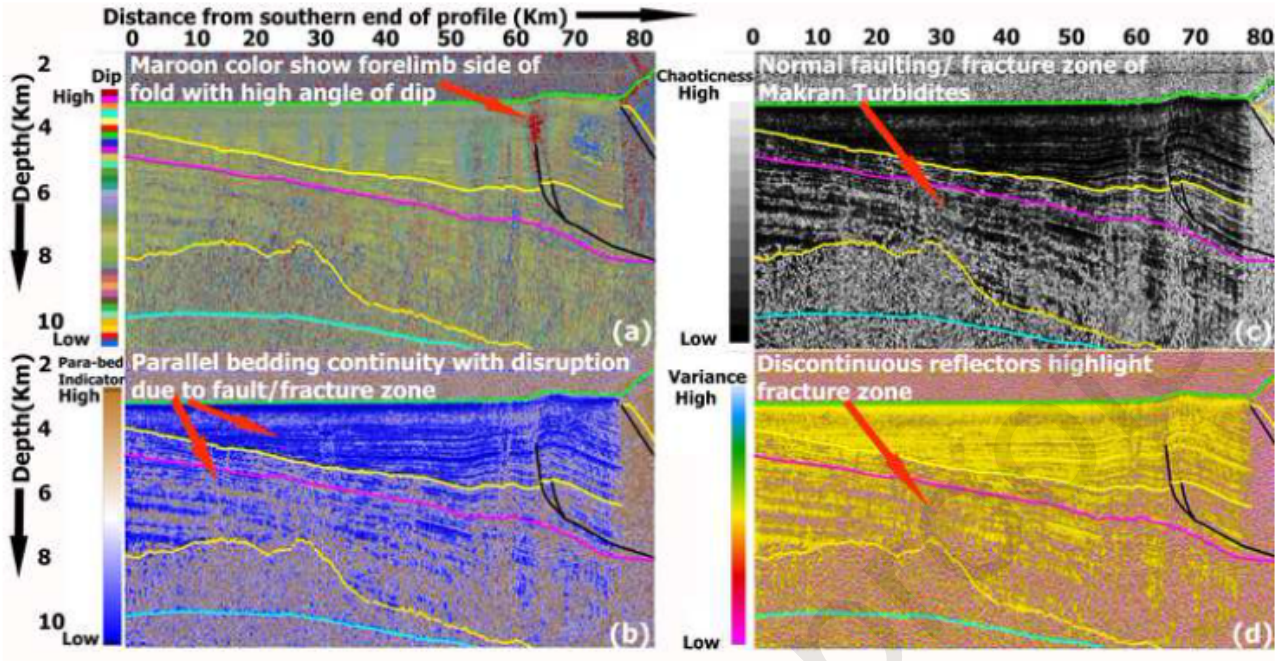

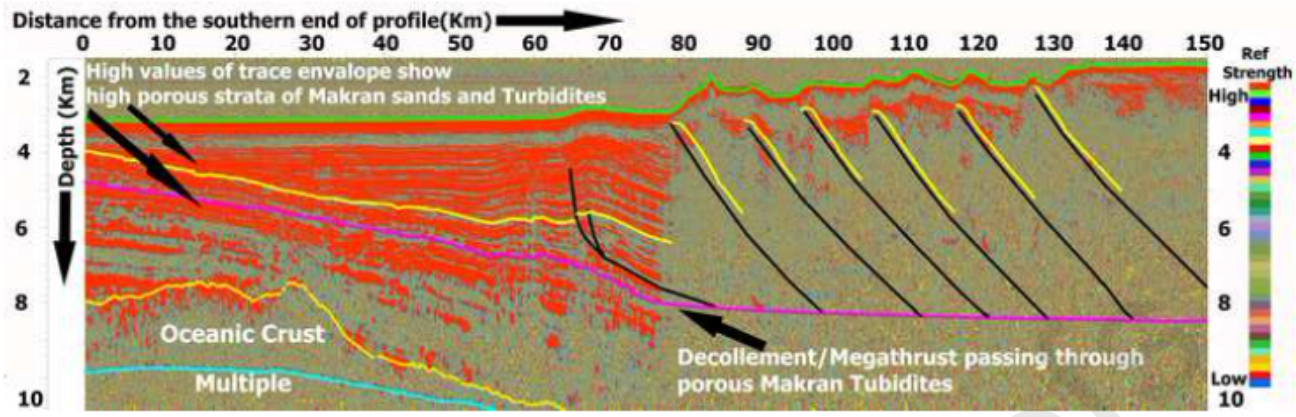

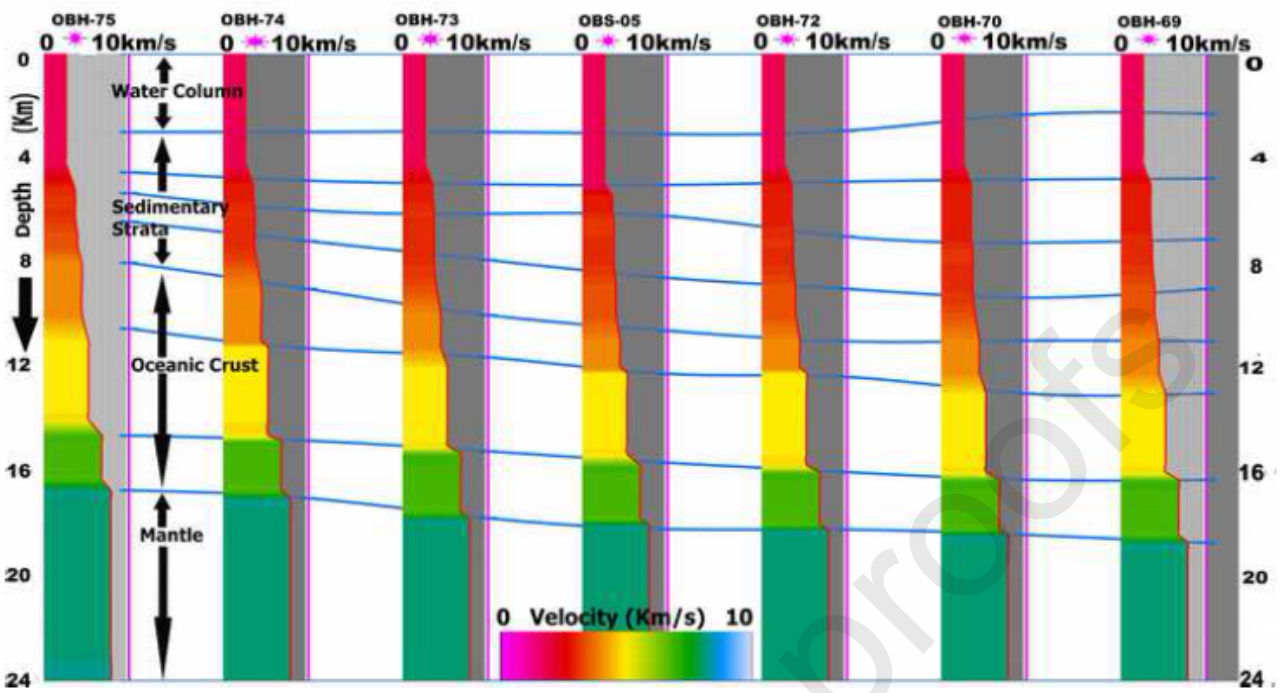

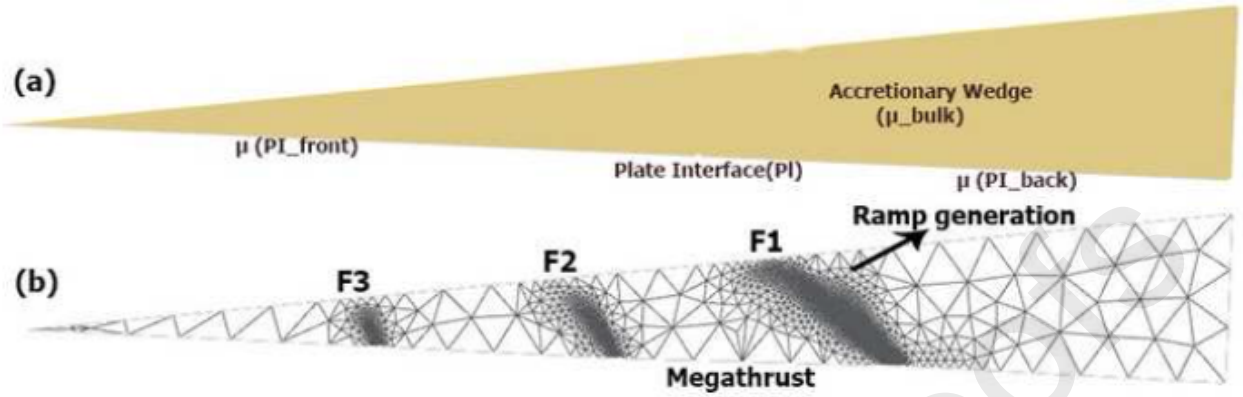

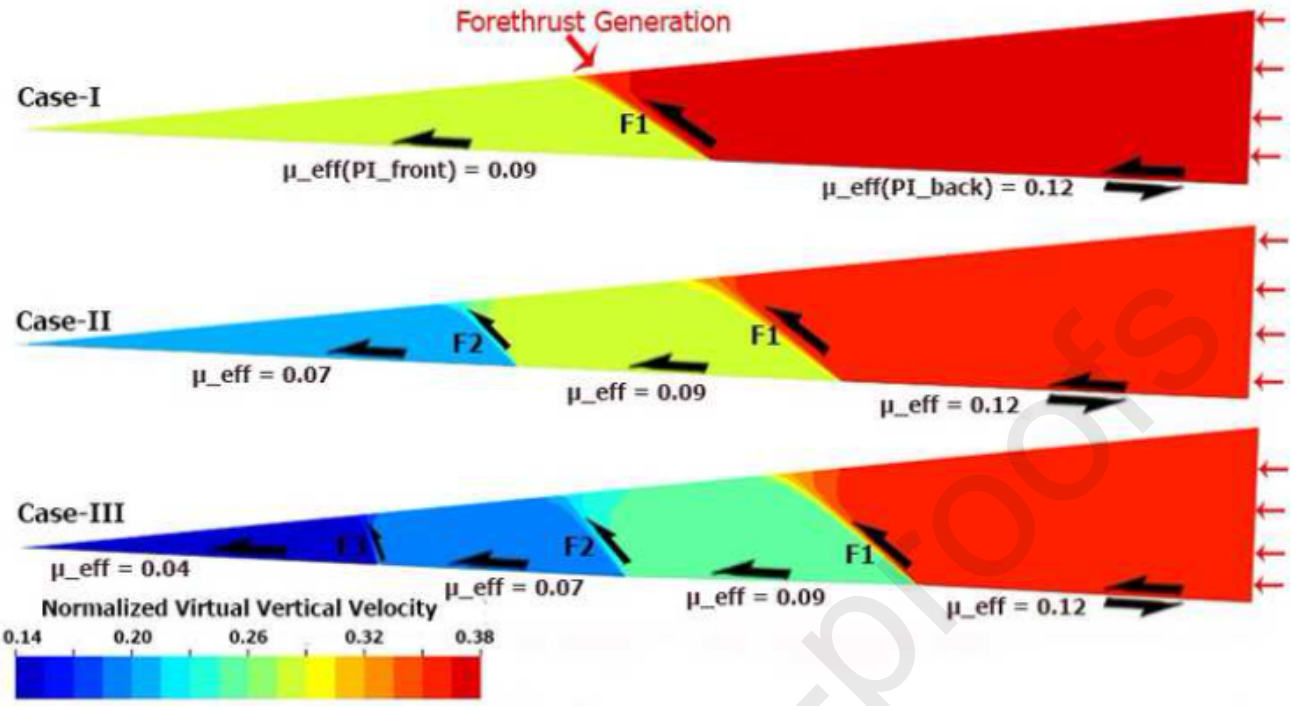

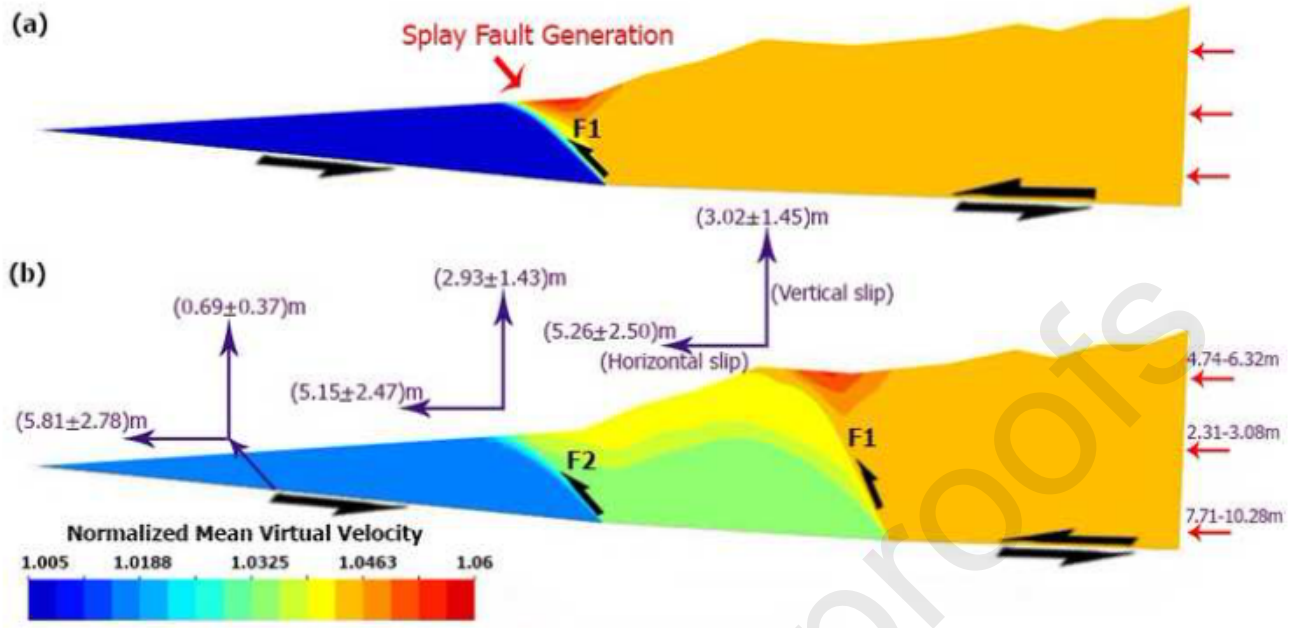

Scenario	Effective friction at Pl_back ($\mu_{eff\_PI\_back}$)	Effective friction at Pl_front ($\mu_{eff\_PI\_front}$)	Remarks
1	>0.12	At any friction no slip occurs	No fault/slip generation due to high values of friction at plate back interface.
2	0.12	0.14, 0.13 or 0.12	Backthrust geometry
3	0.12	0.09, 0.07, 0.04, 0.01…	Forethrust geometry, but as the difference in friction values increases, the steepness of the fault plane increases until it turns to a normal fault.
4	0.12	0.11	Low angle forethrust due to smaller difference in friction values. In this case the fault plane has not developed properly.
5	0.12 (φ =18)	0.01 (φ =2)	Normal fault when there is a very large difference in friction values.

S.no	PI	F1	F2	Remarks
1	δx (m) = 5.81±2.78 δy (m) = 0.69±0.37	5.26±2.50 3.03±1.45	5.15±2.47 2.93±1.43	Figure 8b ($\mu^{eff}_{PI\_back} = 0.12$) & ($\mu^{eff}_{PI\_front} = 0.09, 0.07,$ 0.04 etc.) and range of slip accumulation is 2.31-3.08 m, 4.74-6.32 m, 7.71-10.28 m, for 77, 158 and 257 years, respectively.

Declaration of interests

☒ The authors declare that they have no known competing financial interests or personal relationships that could have appeared to influence the work reported in this paper.

☐The authors declare the following financial interests/personal relationships which may be considered as potential competing interests:

Author Agreement Statement

We the undersigned declare that this manuscript is original, has not been published before and is not currently being considered for publication elsewhere.

We confirm that the manuscript has been read and approved by all named authors and that there are no other persons who satisfied the criteria for authorship but are not listed. We further confirm that the order of authors listed in the manuscript has been approved by all of us.

We understand that the Corresponding Author is the sole contact for the Editorial process. He is responsible for communicating with the other authors about progress, submissions of revisions and final approval of proofs.

Signed by all authors as follows:

Shaukat Parvaiz (corresponding author)

parvaiz_geo@hotmail.com; Shaukat.Parvaiz@buitms.edu.pk

Author statements

Mr. Shaukat Parvaiz perceived the idea and partially executed this idea of the research as well as his contribution in terms of collection of the literature and raw data. Dr. Aamir Ali took the idea and proposed the methodology and implemented along with interpretation and finalization of the manuscript. Dr. Farhan Javed has given support in terms of modern research methods and helped in the interpretation of the data. Dr. Muhammad Ali Shah given the data support and computed the maps.

Highlights

- The Makran subduction zone has an imbricate thrust fault system.
- Attribute analyses show Makran turbidities are fractured under high pore pressures.
- Lateral continuity is observed in the frontal region via velocity analysis.
- Effective friction 0.04-0.12 is required to reproduce the observed fault system.
- Splay faults with high uplift values can amplify earthquake related tsunami.